The Cryosphere

Supplement of

Spatially distributed snow depth, bulk density, and snow water equivalent from ground-based and airborne sensor integration at Grand Mesa, Colorado, USA

Tate G. Meehan et al.

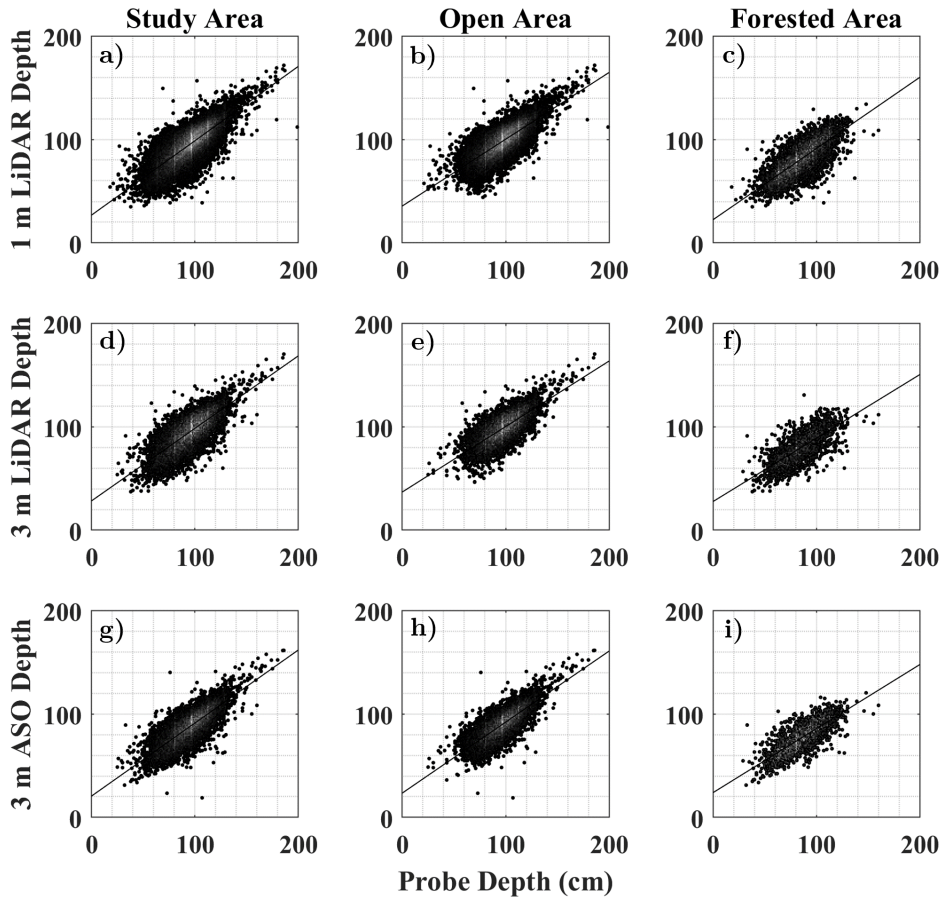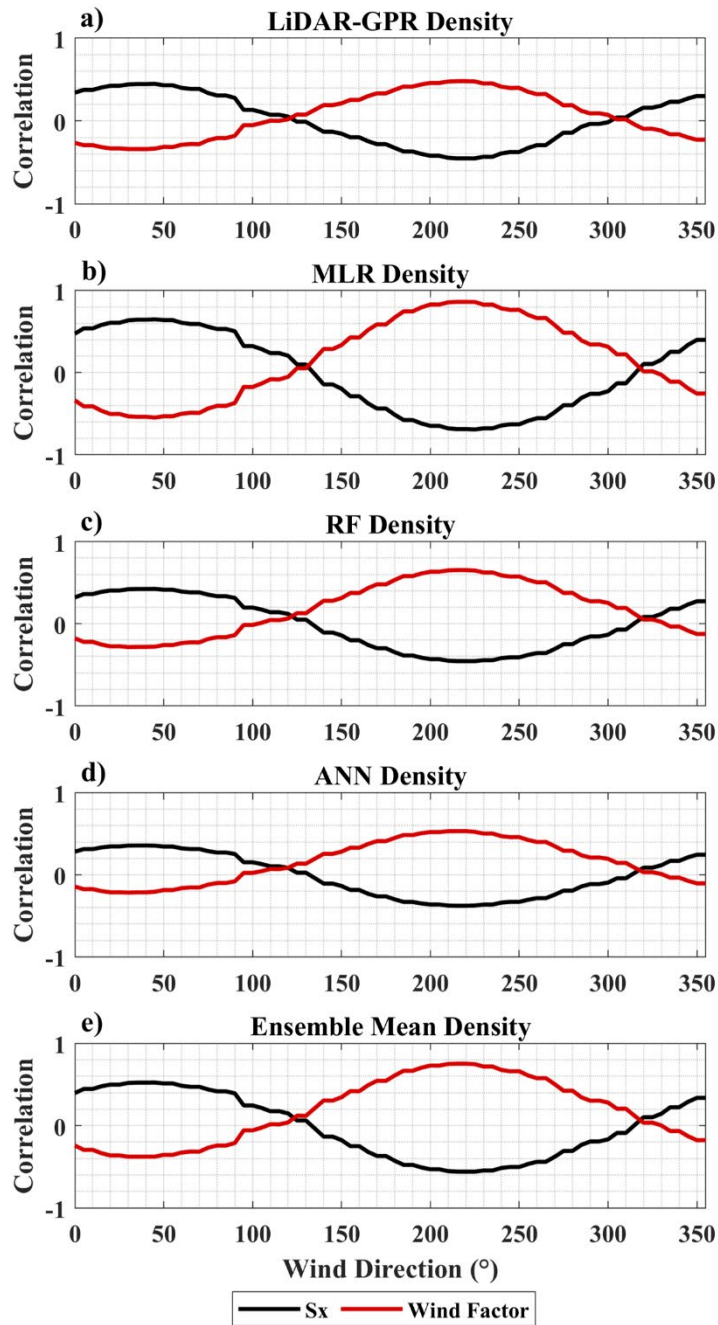*Correspondence to:* Tate G. Meehan (tate.g.meehan@erdc.dren.mil)

Figure S1: Scatter plots comparing validation probe data to the 1 m LiDAR product derived in this work (a – c), upscaled to 3 m (d – f), and ASO 3 m resolution snow depths throughout the entire study area and in open or forested areas separately.

Figure S2: Strong prevailing south-southwest winds (180° – 220°) provide a causal physical mechanism for correlations between the maximum upwind slope (Sx) and wind factor parameters calculated in 5-degree increments.
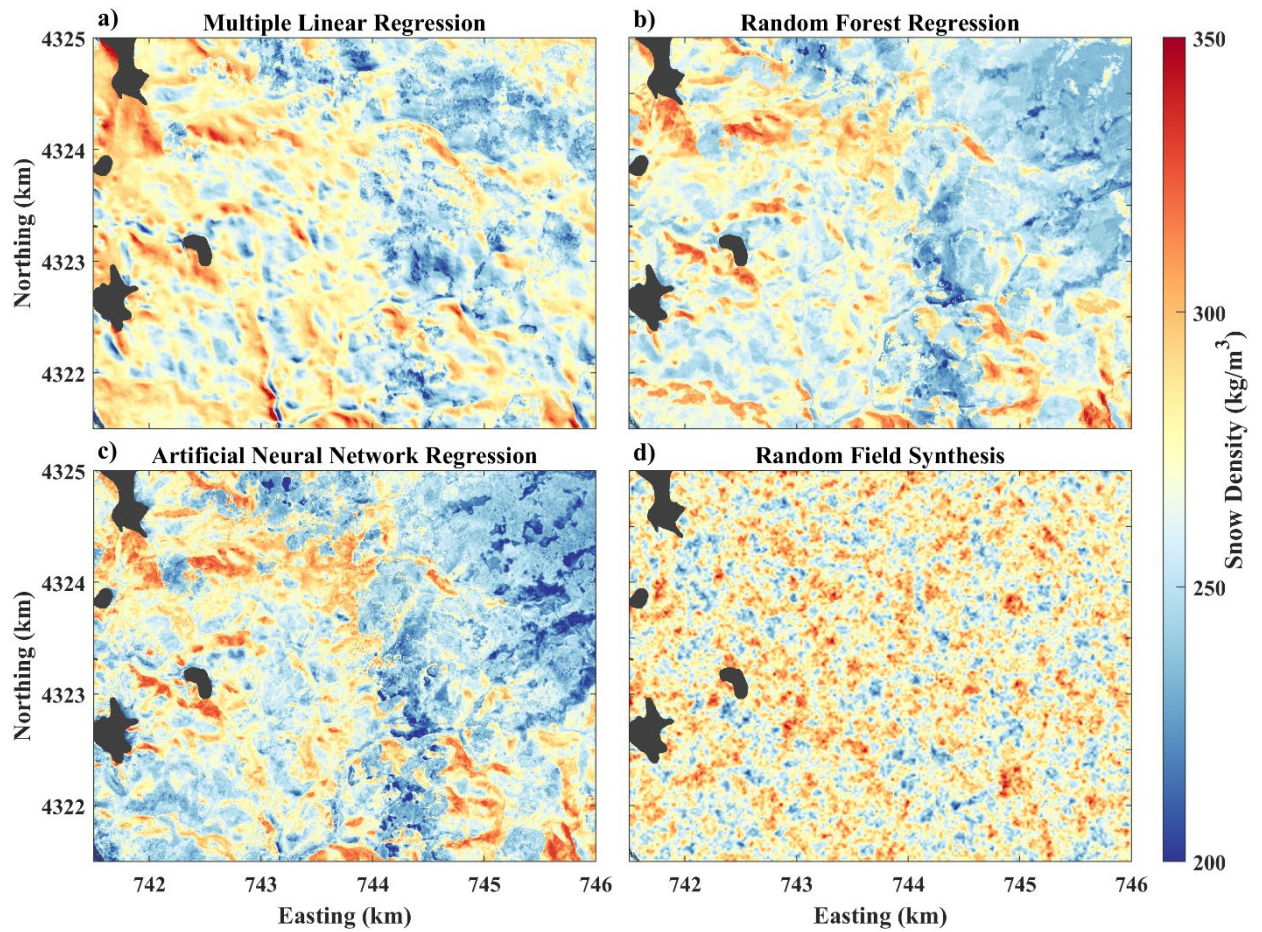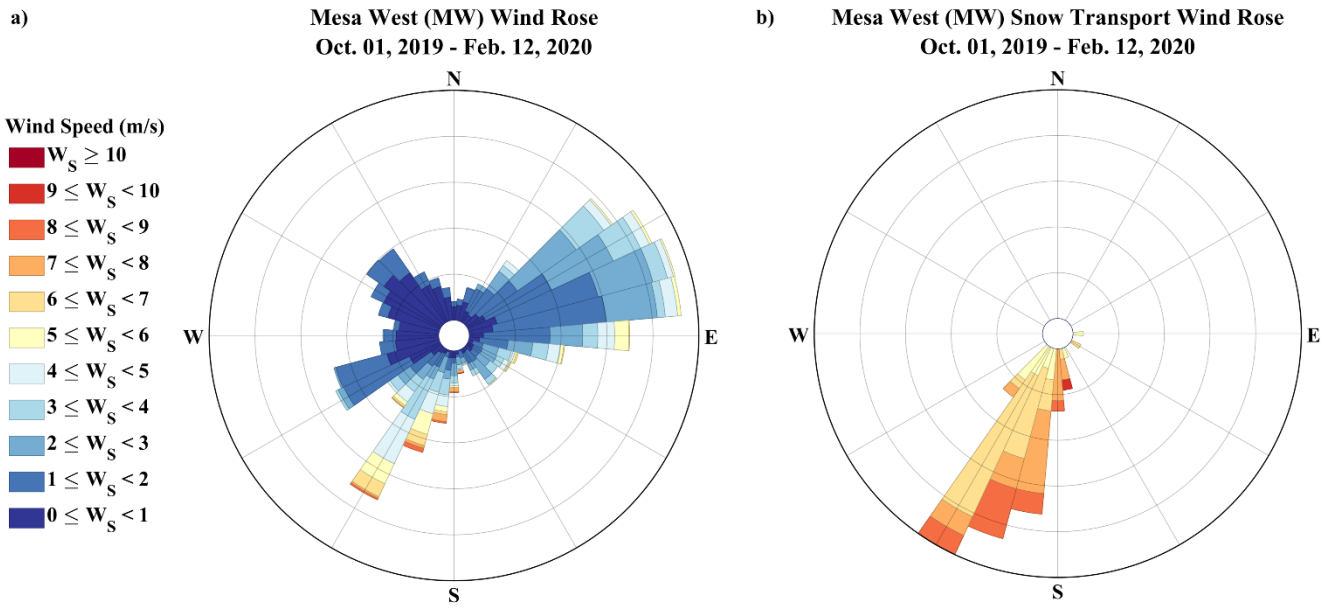
2

Figure S3: Snow density was distributed spatially using regression techniques a) MLR, b) RF, and c) ANN based on predictive features that were derived solely from LiDAR information (i.e. snow depth, elevation, slope, aspect, and vegetation) and d) a synthesised random field model from the statistics of in situ density measurements (275 ± 20 kg/m^3) and the correlation length of snow density estimated via variogram analysis. The colourmap is centred on the mean value 275 kg/m^3.

10

a) Mesa West (MW) Wind Rose
Oct. 01, 2019 - Feb. 12, 2020

b) Mesa West (MW) Snow Transport Wind Rose
Oct. 01, 2019 - Feb. 12, 2020

Wind Speed (m/s)
$W_S \geq 10$
$9 \leq W_S < 10$
$8 \leq W_S < 9$
$7 \leq W_S < 8$
$6 \leq W_S < 7$
$5 \leq W_S < 6$
$4 \leq W_S < 5$
$3 \leq W_S < 4$
$2 \leq W_S < 3$
$1 \leq W_S < 2$
$0 \leq W_S < 1$

Figure S4: Wind speed and direction data from the Mesa West meteorological station (Houser et al., 2022). a) wind rose spanning the beginning of the hydrological year through the end of the SnowEx IOP. b) wind rose of winds that are strong enough to transport snow (Li & Pomeroy, 1997) spanning the beginning of the hydrological year through the end of the SnowEx IOP. The median wind direction for snow transport is 200˚.
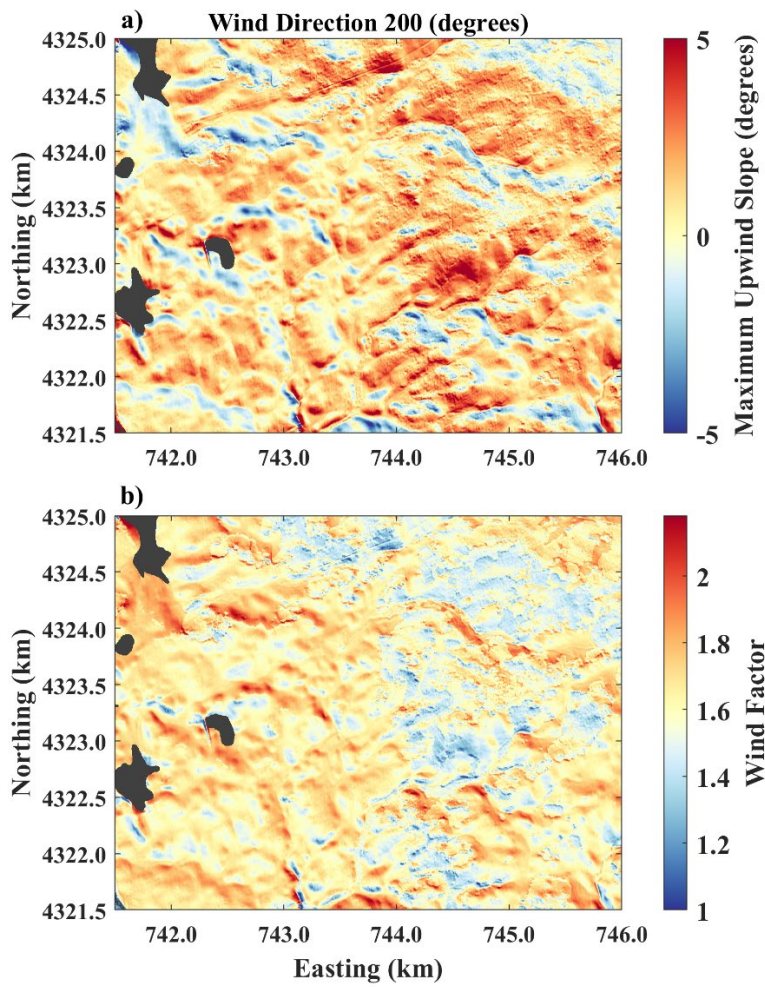
15

4

Figure S5: a) Maximum upwind slope (Sx) and b) wind factor calculated at 200 degrees wind direction.
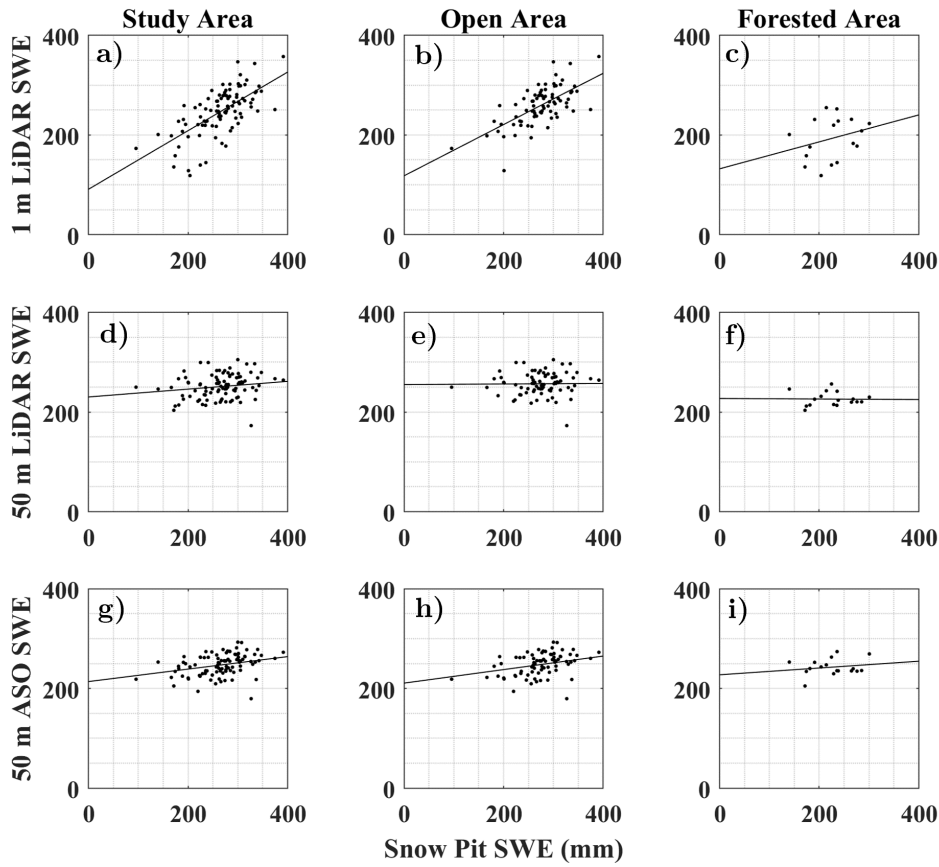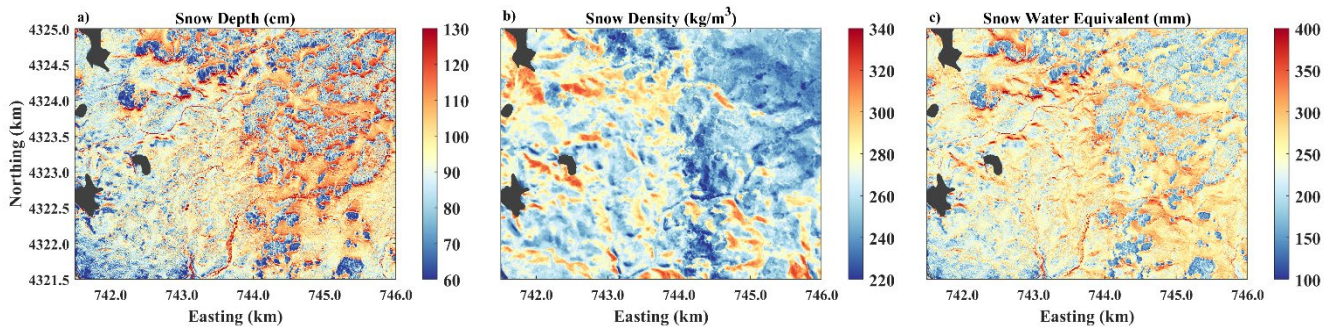
20

Figure S6: Scatter plots comparing validation snow pit SWE data to the 1 m LiDAR product derived in this work (a – c), upscaled to 50 m (d – f), and ASO 50 m resolution SWE product throughout the entire study area and within open or forested areas separately.

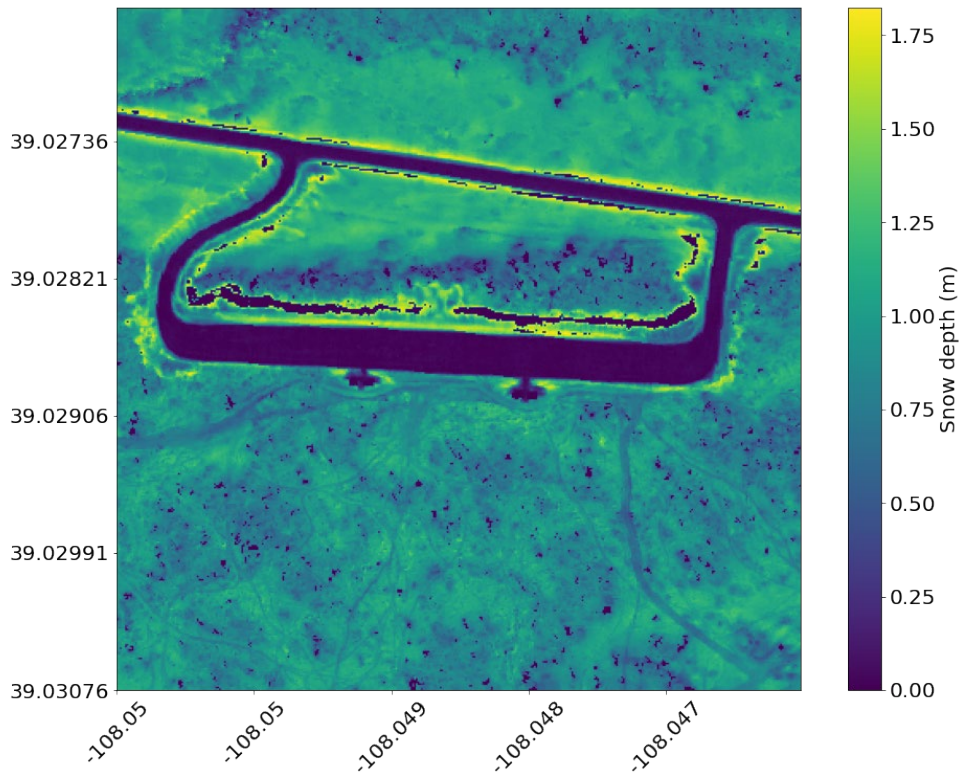**Figure S7: a) $H_{s,LiDAR}$, b) $\rho_{s,\overline{Ens}}$, c) $b_{s,LiDAR-\overline{Ens}}$**

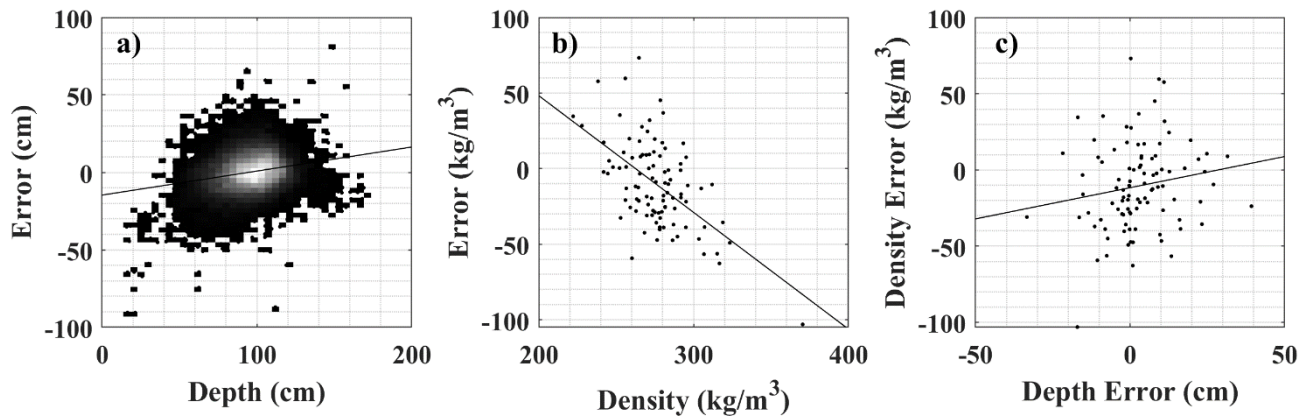**Figure S8: Snow depth values (H$_{s,LiDAR}$) on the ploughed road are between 0 an 5 cm.**

Figure S9: a) Validation snow depth and LiDAR snow depth error (R^2 = 0.04, Bias = 3 cm). b) Validation snow density from 96 pits and machine learning ensemble error (R^2 = 0.35, Bias = -10 kg/m^3). c) The errors in depth and density are uncorrelated (R^2 = 0.03).
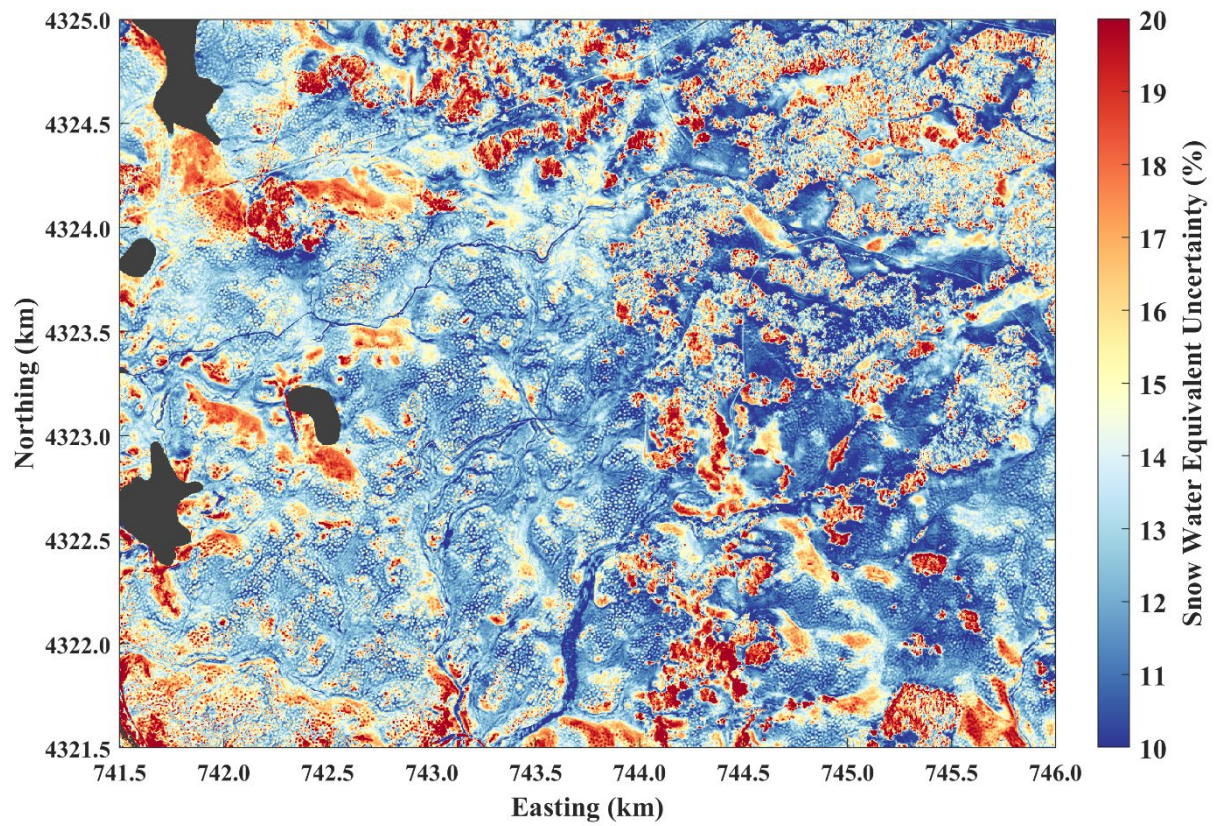
Figure S10: Relative uncertainty in snow water equivalent from propagating the errors in Fig. S9.
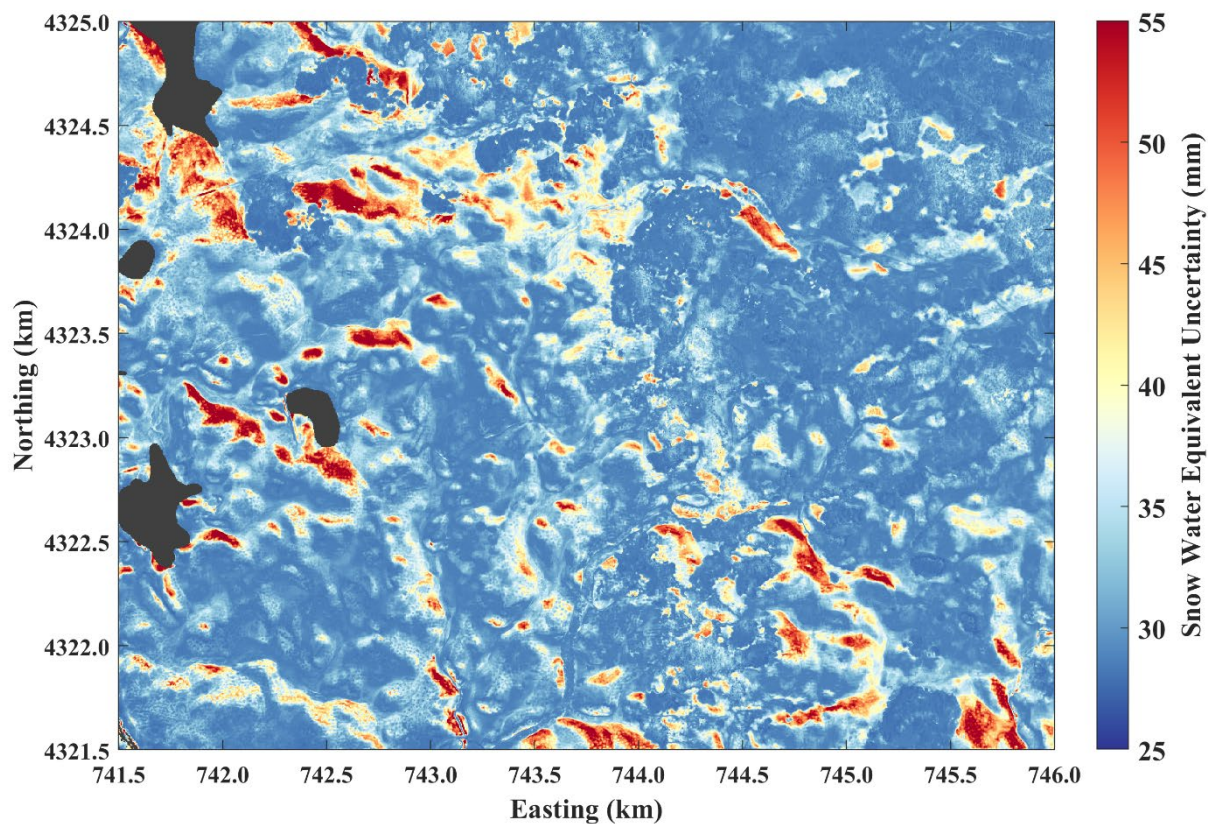
Figure S11: Absolute uncertainty in snow water equivalent from propagating the errors in Fig. S9.

35

Table S1: Comparisons between probed validation data (Table 1 a), LiDAR snow depth products developed in this manuscript, and ASO snow depths.

Snow Depth (cm) Method	All Domain μ ± σ | R² | RMSE |Bias	Open Domain μ ± σ| R² | RMSE | Bias	Forested Domain μ ± σ | R² | RMSE | Bias
ASO ($H_{s,ASO}$)	88 ± 15 | 0.64 | 13 | -7	90 ± 14 | 0.61 | 12 | -7	76 ± 16 | 0.61 | 14 | -8
$H_{s,LiDAR}$ (1 m)	95 ± 16 | 0.61 | 11 | 0	99 ± 14 | 0.57 | 11 | 1	81 ± 16 | 0.60 | 12 | -4
$H_{s,LiDAR}$ (3 m)	95 ± 16 | 0.58 | 12 | 0	99 ± 14 | 0.55 | 11 | 1	80 ± 16 | 0.54 | 14 | -5

Table S2: The maximum correlation and wind direction between snow density and the maximum upwind slope (Sx) and wind factor parameters. Data corresponds to Fig. 7.

Snow Density Method	Sx		Wind Factor	
	R	Direction	R	Direction
LiDAR – GPR	-0.45	225	0.48	220
MLR	-0.69	225	0.86	220
RF	-0.46	225	0.65	215
ANN	-0.38	220	0.53	220
ML Ensemble	-0.56	225	0.75	220
Random Field	-0.03	180	0.02	170

Table S3: Variogram parameters are overviewed for the forested and open areas of Grand Mesa. a) The nugget indicates the percentage amount of measurement variability relative to the mean between co-located observations. b) The sill indicates the percentage variability relative to the mean at which measurements are no longer correlated (coefficient of variation). c) The correlation length is the distance in metres above which measurements are no longer correlated.

a)

Variogram Parameter: Nugget (% of mean)	Open Domain $\mu \pm \sigma$	Forested Domain $\mu \pm \sigma$
Depth ($h_{s,LiDAR}$)	$9 \pm 0\,\%$	$11 \pm 2\,\%$
Density ($\rho_{s,LiDAR-GPR}$)	$2 \pm 0\,\%$	$2 \pm 0\,\%$
SWE ($b_{s,LiDAR-GPR}$)	$13 \pm 0\,\%$	$33 \pm 1\,\%$
TWT ($\tau_{s,GPR}$)	$14 \pm 0\,\%$	$31 \pm 1\,\%$

b)

Variogram Parameter: Sill (% of mean)	Open Domain $\mu \pm \sigma$	Forested Domain $\mu \pm \sigma$
Depth ($h_{s,LiDAR}$)	$26 \pm 0\,\%$	$51 \pm 2\,\%$
Density ($\rho_{s,LiDAR-GPR}$)	$18 \pm 0\,\%$	$14 \pm 0\,\%$
SWE ($b_{s,LiDAR-GPR}$)	$33 \pm 1\,\%$	$47 \pm 1\,\%$
TWT ($\tau_{s,GPR}$)	$26 \pm 0\,\%$	$45 \pm 0\,\%$

c)

Variogram Parameter: Correlation Length (m)	Open Domain $\mu \pm \sigma$	Forested Domain $\mu \pm \sigma$
Depth ($h_{s,LiDAR}$)	71 ± 4	17 ± 2
Density ($\rho_{s,LiDAR-GPR}$)	95 ± 2	97 ± 4
SWE ($b_{s,LiDAR-GPR}$)	99 ± 5	88 ± 17
TWT ($\tau_{s,GPR}$)	105 ± 6	64 ± 5

Table S4: Comparisons between snow pit validation SWE data (Table 4 a), LiDAR SWE products developed in this manuscript, and ASO 50 m resolution SWE.

SWE (mm) Method	All Domain $\mu \pm \sigma$ | R^2 | RMSE | Bias	Open Domain $\mu \pm \sigma$ | R^2 | RMSE | Bias	Forested Domain $\mu \pm \sigma$ | R^2 | RMSE | Bias
ASO ($b_{s, ASO}$)	248 ± 22 | 0.10 | 57 | -21	249 ± 22 | 0.11 | 59 | -30	243 ± 16 | 0.03 | 47 | 17
$b_{s, LiDAR-\overline{Ens}}$ (1 m)	245 ± 53 | 0.56 | 46 | -20	259 ± 41 | 0.61 | 42 | -18	198 ± 57 | 0.19 | 56 | -27
$b_{s, LiDAR-\overline{Ens}}$ (50 m)	251 ± 24 | 0.03 | 60 | -18	256 ± 23 | 0.0 | 63 | -22	226 ± 14 | 0.0 | 60 | 1